1968 Heat Transfer Fluid Mechanics Institute, Stanford University Press, pp. 3–17.

[14] Sternberg, J., "A Theory for the Viscous Sublayer of a Turbulent Flow," *Journal of Fluid Mechanics*, Vol. 13, 1962, pp. 241–271.

[15] Schubert, G. and Corcos, G. M., "The Dynamics of Turbulence Near a Wall According to a Linear Model," *Journal of Fluid Mechanics*, Vol. 29, 1967, pp. 113–135.

[16] Jenkins, R., "Variation of the Eddy Conductivity with Prandtl Modulus and its Use in Prediction of Turbulent Heat Transfer," Heat Transfer and Fluid Mechanics Institute, Stanford University Press, 1951, pp. 147–158.

NOVEMBER 1971 AIAA JOURNAL VOL. 9, NO. 11

Parametric Study of a Two-Dimensional Turbulent Wall Jet in a Moving Stream with Arbitrary Pressure Gradient

SURESH H. GORADIA* AND GENE T. COLWELL†
Georgia Institute of Technology, Atlanta, Ga.

Measurements of flow parameters for a two-dimensional turbulent wall jet are presented in a range of ratios of slot stream velocity to external stream velocity with pressure gradients, not previously investigated. These data are utilized for the calculations of wall shear and shear distribution by numerical methods. Relationships among the parameters are considered.

Nomenclature

C_p = pressure coefficient
$f(\eta_1)$ = similarity function for velocity profile in the jet layer in initial region
$f(\eta_2)$ = similarity function for velocity profile in the wake layer in the initial region
$f(\eta_3)$ = similarity function for velocity profile in the jet layer in main region
$f(\eta_4)$ = similarity function for velocity profile in the wake layer in the main region
H = form factor or pressure gradient parameter
$\tilde{H}$ = ratio of dissipation energy thickness and momentum thickness
M = Mach number
P_{ST} = wall static pressure, lbf/ft²
P_T = Pitot tube total pressure, lbf/ft²
P_∞ = freestream pressure lbf/ft²
$R_{e\theta}$ = Reynolds number based on wall layer momentum thickness
U_c = velocity in the core layer in the initial region, fps
$U_{c(0)}$ = slot velocity at the exit, fps
$U_{e(x)}$ = velocity at the edge of viscous layer, fps
$U_{e(0)}$ = velocity at the edge of viscous layer at the slot exit, fps
$U_{w(x)}$ = velocity at the junction of jet layer and wake layer, fps
$U_{m(x)}$ = velocity at the junction of wall layer and jet layer, fps
U_∞ = freestream velocity, fps
u = X component of velocity in viscous layer, fps
v = Y component of velocity in viscous layer, fps
x = distance measured from slot exit, in.
y = distance measured from wall, in.
y_{1c} = distance y in the wake layer above the wall in initial region for $f(\eta_2) = 0.5$, in.
y_{2c} = distance y in the wake layer above the wall in main region for $f(\eta_4) = 0.5$, in.
δ^* = displacement thickness for wall layer in initial and main region, in. $\int_0^{\delta_1} [1 - (u/U_c)]dy$ or $\int_0^{\delta_5} [1 - (u/U_m)]dy$
δ^{**} = dissipation energy thickness, in. $\int_0^{\delta_1} (u/U_c)[1 - (u/U_c)^2]\,dy$ or $\int_0^{\delta_5} (u/U_m)[1 - (u/U_m)^2]\,dy$
$\delta_1, \delta_2, \delta_3, \delta_4, \delta_5$, etc. = distance shown in Fig. 1, in.
η_1 = similarity parameter for velocity profile in the jet layer in the initial region
η_2 = similarity parameter for velocity profile in the wake layer in the initial region
η_3 = similarity parameter for velocity profile in the jet layer in the main region
η_4 = similarity parameter for velocity profile in the wake layer in the main region
θ = momentum thickness for wall layer in initial region and main region, in. $\int_0^{\delta_1} (u/U_c)[1 - (u/U_c)]dy$ or $\int_0^{\delta_5} (u/U_m)[1 - (u/U_m)]dy$
ρ = density of air, lbm/ft³
τ = shear stress at a distance y above wall, lbf/ft²
τ_w = wall shear stress, lbf/ft²

Received November 11, 1970; revision received May 17, 1971. Considerable credit is due Y. T. Chin and R. F. Tanner of Lockheed Georgia Company, who originally built the majority of the test rig that was used during the course of these experiments. Also, much credit is due T. Dansby, D. M. Ryle, and B. H. Little of Lockheed Georgia Company for their support and advice.

Index category: Boundary Layers and Convective Heat Transfer–Turbulent.

* Graduate Student, School of Mechanical Engineering; also Senior Aerodynamic Engineer, Lockheed Georgia Company, Marietta, Ga.

† Associate Professor, School of Mechanical Engineering.

Introduction

THE behavior of wall jets is of practical interest because of their application in film cooling or heating and in boundary-layer control on airfoil sections and wings of STOL aircraft. Detailed experimental investigations have been carried out by prominent investigators such as Bradshaw and Gee,[1] Kruka and Eskinazi,[2] Myers et al.,[3] Hubbart and Bangart,[4] Birkebak et al.,[5] and Kacker and Whitelaw.[6] Some of the investigators concentrated their efforts on very

high values of velocity ratio $U_{c(0)}/U_{e(0)}$, some confined their attention to flow without pressure gradient, some did not consider the initial region where the core flow exits, and some confined their attention to slot exit velocity corresponding to Mach numbers near unity when flow cannot be analyzed according to incompressible assumptions. The reason for concentration by the individual investigators on higher velocity ratios and on flow without pressure gradient is quite understandable, since in these cases the velocity profile beyond the initial region is composed of two layers only. This type of flow then can be analyzed approximately by methods of similarity.

The present paper describes detailed behavior of the viscous flow, its mean properties, and the relation between various boundary-layer physical parameters for a two-dimensional, incompressible wall jet flow in a moving stream and in the presence of various pressure gradients of practical interest. The measurements are confined to velocity ratios $U_{c(0)}/U_{e(0)}$ in the neighborhood of 1 to approximately 2.0. The measurements are performed from the exit of the slot to approximately 160 slot heights downstream. The spacing between two X locations where the velocity profiles were measured was kept small for two purposes, namely, 1) to determine accurately the beginning and end of various regions shown in Fig. 1, and 2) to determine accurately the relation between various physical parameters of importance by the use of numerical methods with the aid of digital computers. The measurements for zero pressure gradient and velocity ratios greater than one were performed to check experimental results with other investigators such as Kruka and Eskinazi,[2] Kacker and Whitelaw,[6] and Patel and Newman.[7] The measurements for zero pressure gradient and velocity ratio less than one were done with a view to supplement the investigation of effectiveness of film cooling results performed by Hartnett et al.[5] and also by Seban and Back.[15]

The primary purpose of the present investigation is to study downstream development of the viscous flow when flow through the slot, with initial boundary layer, mixes with the parallel stream, also having initial boundary layer, in the presence of adverse pressure gradient. When the initial velocity ratio is such that $1 \leq U_{c(0)}/U_{e(0)} \leq 1.7$, then the wake layer shown in Fig. 1 exists quite far downstream of slot exit. This complex flow has not been studied in detail previously, even though it exists on multicomponent airfoils. This paper reports the results of measurements of velocity profiles and investigations of the relations among important physical parameters. Establishment of relations between physical parameters is of vital importance in the solution of this type of viscous flow on airfoil surfaces by integral techniques.

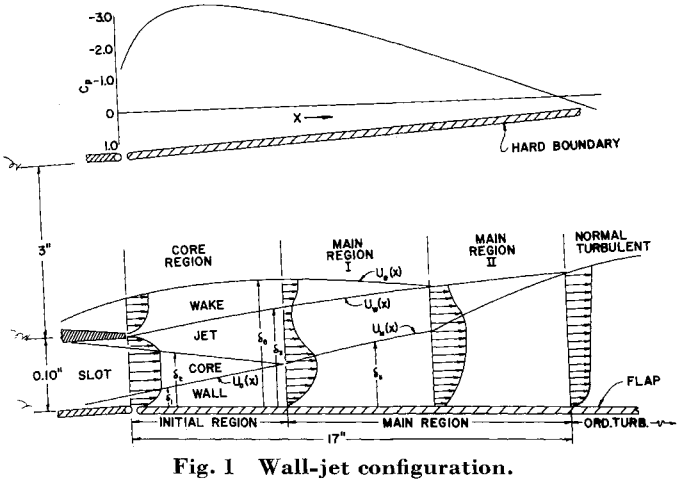

Fig. 1 Wall-jet configuration.

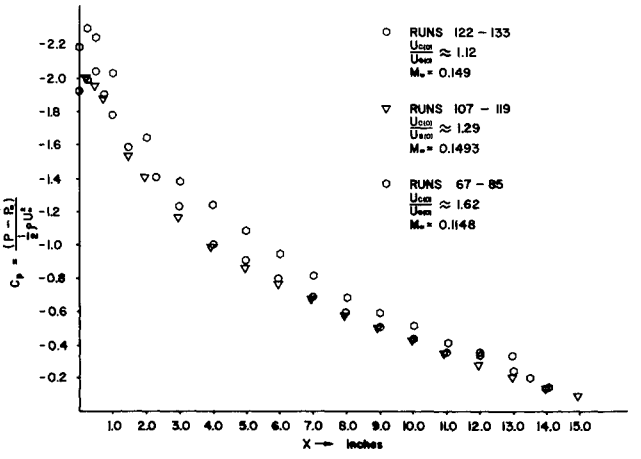

Fig. 2 Pressure distribution for initial velocity ratios of 1.12, 1.29, and 1.62.

Related Investigations

Glauert[8] used a similarity solution approach for the solution of the wall jet in a still medium. Based on physical reasoning in this simpler type of flow, he was the first to postulate that the entire flowfield of the wall jet cannot conform to one over-all similarity solution. He divided the flow into wake layer and jet layer on either side of maximum velocity and treated the two regions separately. Myers et al.[3] conducted an analytical and experimental study of the wall jet with no external stream. They treated the flow in both initial region and main region by integral methods. The velocity profile was divided into wall layer and jet layer. The velocity profile in the wall layer was assumed of the $\frac{1}{7}$th power law type, and the velocity profiles in the outer layer were assumed to be similar, having the same similarity function as for a free jet. The wall shearing stress was measured by a hot film technique, and the results were generalized as a function of Reynolds number and slot height. Kruka and Eskinazi[2] have studied experimentally and analytically wall jet flow with an external stream at a large distance from slot exit. The ratios of injection to freestream velocity considered by these authors were greater than 2.5, and only zero pressure gradient was considered. The flow was again divided into inner and outer layers, and similar velocity profiles were found to exist in both layers. Experimentally, the friction factor was found to be proportional to the inner Reynolds number raised to a power and consequently not constant with x. Thus,

$$C_f = K_1[U_m\delta_1/\nu]^{K_2}$$

where K_1 and K_2 are constant but depend on the initial velocity ratio. Good agreement was found between calculated shear stress distribution across the viscous layer and that experimentally determined from Preston probe and hot-wire anemometer readings. Kacker and Whitelaw[6] investigated wall jet flow experimentally for zero pressure gradient and in the range of velocity ratios of 0.75–2.74. Measurements were made of mean velocity profiles and turbulent shear distribution across the viscous layer. It was found that the shear work integral decreases exponentially for flows with velocity maxima and that the point of zero shear was closer to the wall than that of zero velocity gradient. The characteristic of the shear distribution profile measured by these authors is similar to the one calculated numerically under the present investigation. The authors obtained the values of skin friction coefficient at a distance greater than 50 slot heights from the slot exit by the use of Clauser[14] charts, in which the constant shear lines are plotted from the equation

$$U^+ = K^{-1}\ln(y^+) + c$$

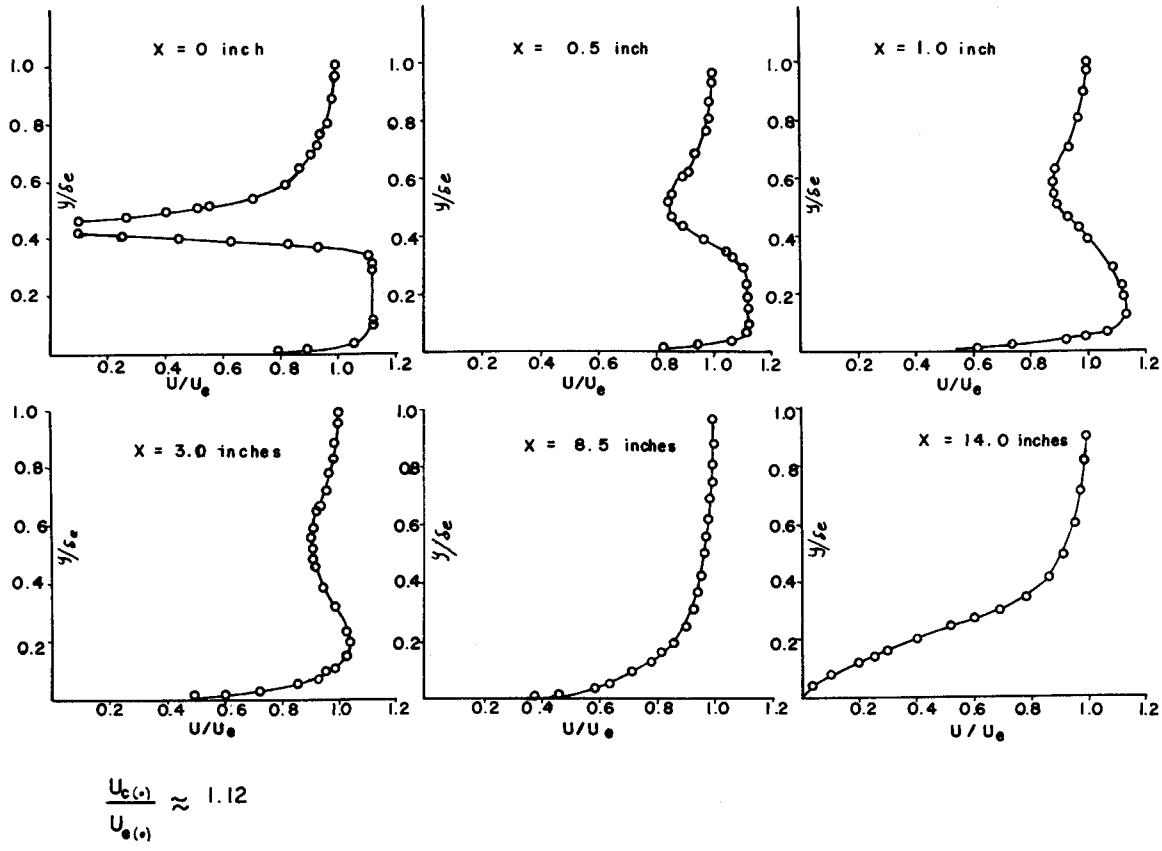

Fig. 3 Velocity profiles for initial velocity ratio of 1.12.

where

$$U^+ = u/(\tau_w/\rho)^{1/2} \qquad y^+ = y(\tau_w/\rho)^{1/2}/\nu$$

and K and C are constants.

Bradshaw and Gee[1] conducted experiments on wall jets in still air on flat and curved surfaces and beneath an external stream. They measured the wall shear for the case of no external stream and without any pressure gradient and formulated an expression for it as a function of Reynolds number based on peak velocity at the edge of the wall layer and wall layer thickness. Thus,

$$\tau_w/\tfrac{1}{2}\rho U_m^2 = 0.0315[U_m\delta_1/\nu]^{-0.182}$$

They found that Reynolds shear stress was not zero at the velocity maximum, thus invalidating the simple assumptions of layer independence made by other workers.

Escudier and Whitelaw[16] reported results on boundary layers with adverse pressure gradients of injecting secondary flow normal to the main stream through a strip of porous material placed across the test plate flush with its surface. The authors reached the conclusion that pressure gradient has relatively little influence on effectiveness up to the condition of separation. Their conclusion seems to be in agreement with results reported by Hartnett et al.[5] and by Seban and Back.[15,19]

Nicoll and Whitelaw[17] investigated the wall jet in the range of slot to freestream velocity from 0.467–2.26 using helium as a tracer gas. The authors proposed a prediction technique that gives good correlation with experimental data when the upstream boundary layer is small and at a distance greater than 10 slot heights downstream of slot exit.

Table 1 Designation of experimental runs

Case	Runs	$M_{e(0)}$	$M_{c(0)}$	$\frac{M_{c(0)}}{M_{e(0)}}$	δ flap, deg	δ plate, deg	Pressure gradient
1	1–24	0.1	0.3	3.0	0	...	Zero
2	25–43	0.2	0.3	1.57	0	...	Zero
3	48–66	0.23	0.17	0.74	0	...	Zero
4	67–85	0.195	0.325	1.67	3	3	Mild adverse
5	86–96	0.25	0.425	1.7	4	4	Mild adverse
6	97–106	0.25	0.185	0.74	4	4	Medium adverse
7	107–119	0.25	0.325	1.3	7	7	High adverse
8	122–133	0.25	0.28	1.12	7	7	High adverse

Experimental Facility

Figure 1 shows schematically the geometry of the test section, along with important over-all dimensions. Measurements were confined to the range of velocities through both the slot and freestream at slot exit where the flow can be considered incompressible. The range of the slot velocities at the exit was confined to 120–307 fps, and the range of external stream velocity at the exit of slot was confined to 80–250 fps. Desired pressure distribution was obtained by deflecting both the flap and the hard boundary from 0° to approximately 7°. Static pressures were measured both on the flap upper surface and on the surface of the hard boundary. The same values of static pressure were obtained on the flap and the boundary at the same X locations except at approximately 140 slot heights downstream, where local separation was observed. Table 1 shows the list of conditions for which measurements were performed.

Results and Discussion

A computer program was formulated for data reduction and analysis of the experimental data taken under the present investigation. As mentioned previously, experimental measurements consisted of wall static pressures on the flap, wall static pressures on the hard boundary, total pressures across the viscous layer, and ambient temperature and barometric pressures. The foregoing measured information at two

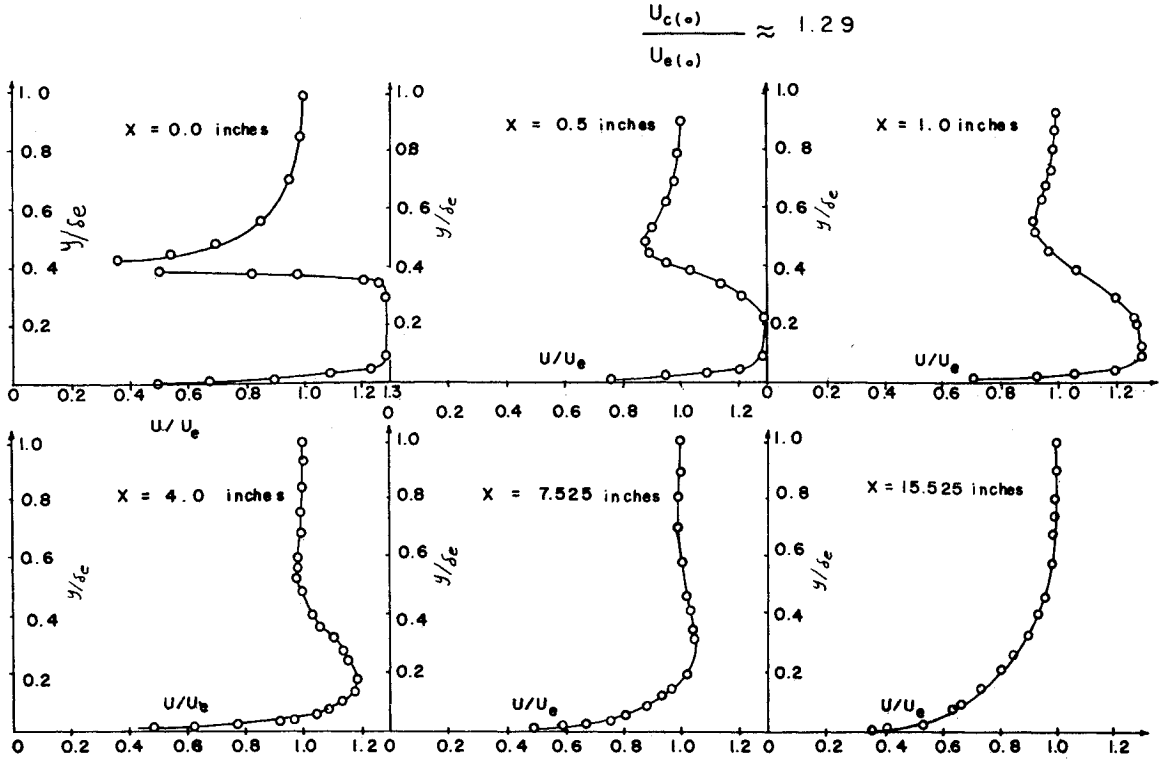

Fig. 4 Velocity profiles for initial velocity ratio of 1.29.

closely spaced X locations constitutes the input to the computer program which calculates the following information: 1) velocity profiles at two stations; 2) wall shear stress between two stations; 3) shear stress distribution across the viscous layer between two stations; 4) for the wall-layer at both the stations Reynolds number based on momentum thickness, displacement thickness, wall layer thickness, form factor H, ratio $\tilde{H}$ of energy thickness δ^{**} and momentum thickness θ; 5) turbulent dissipation for the wall layer and entire viscous layer, wall shear calculated by expressions such as Nash's, Bradshaws, Kruka and Eskinazis, Clauser's, Sigalla's,[12] etc., e.g., for the main region,

$$2\int_0^{\delta_5} \frac{\tau}{\rho u_m^2} \frac{\partial}{\partial y}\left(\frac{u}{u_m}\right) dy$$

and for the initial region,

$$2\int_0^{\delta_1} \frac{\tau}{\rho u_c^2} \frac{\partial}{\partial y}\left(\frac{u}{u_c}\right) dy$$

6) calculated nondimensional velocity profiles for jet layer

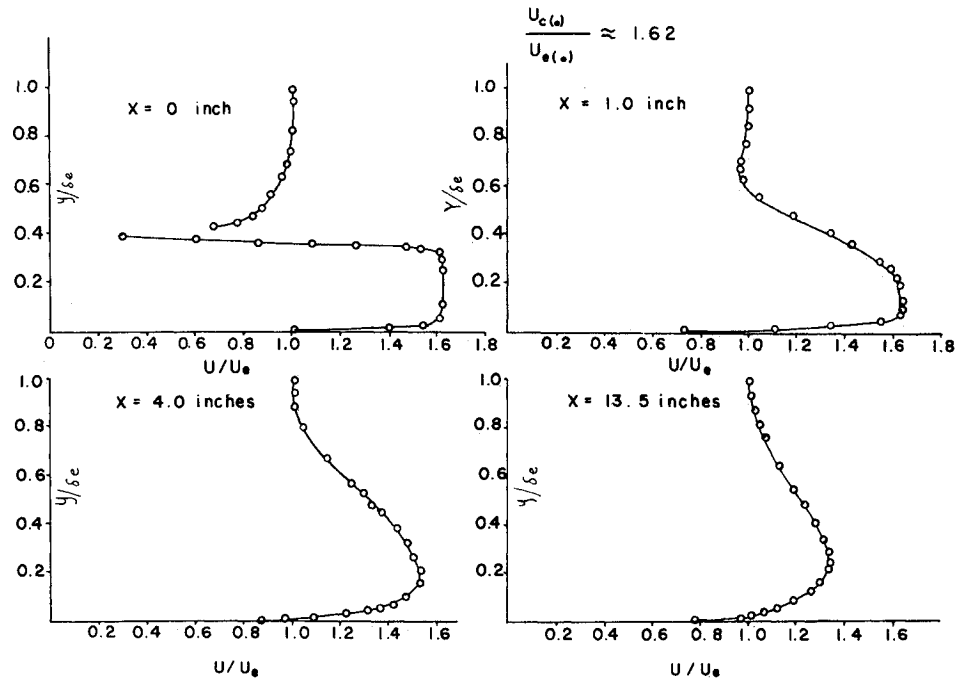

Fig. 5 Velocity profiles for initial velocity ratio of 1.62.

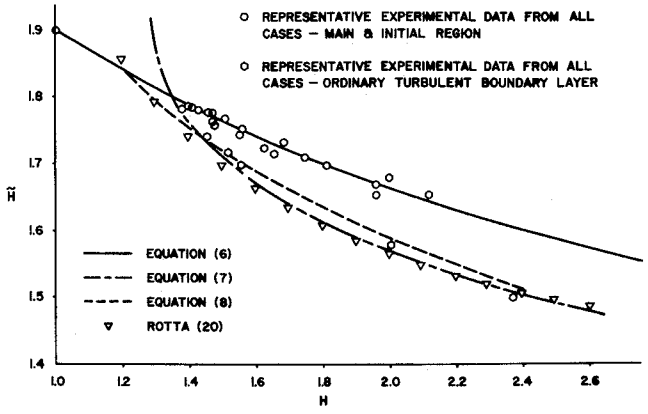

Fig. 6 Relation between H and $\tilde{H}$ for wall layer in the initial and main region and ordinary turbulent boundary layer.

and wake layer at both stations; 7) various integrals at each of stations such as

$$\int_0^{y_1} \frac{u}{U_e}\,dy \qquad \int_0^{y_1} \left(\frac{u}{U_e}\right)^2 dy$$

$$u_{(y_i)} \int_0^{y_1} \frac{u}{U_e}\,dy \qquad u(y_1) \int_0^{y_1} \left(\frac{u}{U_e}\right)^2 dy$$

where y_1 is any distance above wall in the viscous region, and $u(y_1)$ is the velocity at distance y_1 above the wall.

All mean velocities were calculated using the following equation:

$$P_T = P_{ST} + \tfrac{1}{2}\rho u^2 \tag{1}$$

where P_T is Pitot tube total pressure, and P_{ST} is wall static pressure.

The total pressures were measured by means of a probe with external dimensions of approximately 0.007 × 0.03 in. MacMillan's[13] correction was applied to all values of velocities computed by Eq. (1).

In order to calculate the wall shear and shear stress distribution across the viscous layer, use of following basic equations was made:

$$v = -\int_0^y \frac{\partial u}{\partial x}\,dy \tag{2}$$

$$u\partial u/\partial x + v\partial u/\partial y = -(1/\rho)dP/dx + (1/\rho)\partial\tau/\partial y \tag{3}$$

$$\partial P/\partial y = 0$$

and

$$dP/dx = -\rho U_e dU_e/dx \tag{4}$$

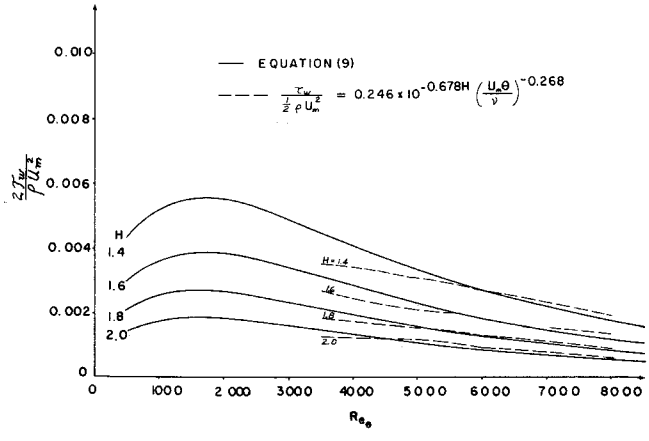

Fig. 7 Wall shear coefficients.

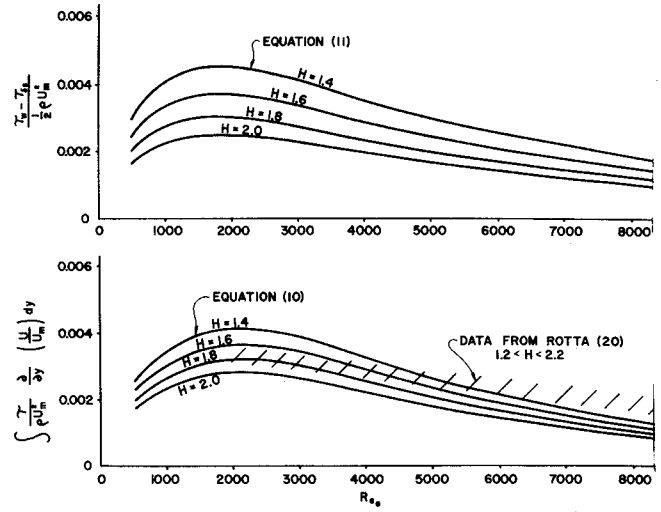

Fig. 8 Difference between wall shear and shear at edge of wall layer and wall-layer dissipation integral.

By integrating Eq. (3) from $y = 0$ to $y = \delta$, making use of Eqs. (2) and (4), and using Leibnitz's rule and integration by parts, the following equation can be derived after some algebraic simplification:

$$U_e^2\left[\frac{d}{dx}\left\{\int_0^{y_1}\frac{u}{U_e}\left(\frac{u}{U_e}-\frac{u(y_1)}{U_e}\right)dy\right\}\right] + \left[U_e\left\{\int_0^{y_1}\frac{u}{U_e}\,dy\right\}\right]\cdot\left[U_e\frac{d}{dx}\left\{\frac{u(y_1)}{U_e}-1\right\}\right] + \left[U_e\frac{dU_e}{dx}\cdot\int_0^{y_1}\left(\frac{u}{U_e}-1\right)dy\right] + 2\left[U_e\frac{dU_e}{Ux}\cdot\int_0^{y_1}\frac{u}{U_e}\times\left(\frac{u}{U_e}-\frac{u(y_1)}{U_e}\right)dy\right] + \left[U_e\int_0^{y_1}\frac{u}{U_e}\,dy\right]\cdot\left[\frac{u(y_1)}{U_e}-1\right]\frac{dU_e}{dx} = \frac{1}{\rho}\left(\tau_{(y_1)}-\tau_w\right) \tag{5}$$

In the preceding equation, the symbols have the following meaning: y_1 = distance above wall; U_e = velocity at edge of viscous layer; $\tau_{(y_1)}$ = shear stress at $y = y_1$; and τ_w = wall shear stress.

The left-hand side of Eq. (5) was programed to compute $(\tau_{(y_1)} - \tau_w)$ at various distances y_1 above the wall. Shear stress was assumed to be zero at very large distances from the wall in order to obtain wall shear. The same equation and the same numerical procedures were used to compute shear distribution, wall shear, and turbulent dissipation for initial regions and main regions for the conditions listed in Table 1.

Figure 2 shows the pressure distribution that was imposed on the viscous flow for case numbers 8, 7, and 4, respectively, shown in Table 1. Here the pressure is plotted as pressure coefficient vs X measured from slot exit in inches. These pressure distributions were obtained by deflecting the flap and hard boundary as shown in Fig. 1. The favorable pressure distribution from slot exit to approximately ½ in. downstream was due to the curvature effect near the knee of the flap. As seen in Fig. 2, the pressure becomes constant near the rear end of the flap where incipient separation was observed.

Figures 3–5 show plots of velocity profiles for cases 8, 7, and 6, respectively, shown in Table 1. These experimental data for the velocity profiles at the various distances downstream of the slot exit are in agreement with the mathematical model of the viscous flow shown in Fig. 1. The length of the initial region for different velocity ratios and different flow conditions and pressure distributions is between 1 and 2 in.,

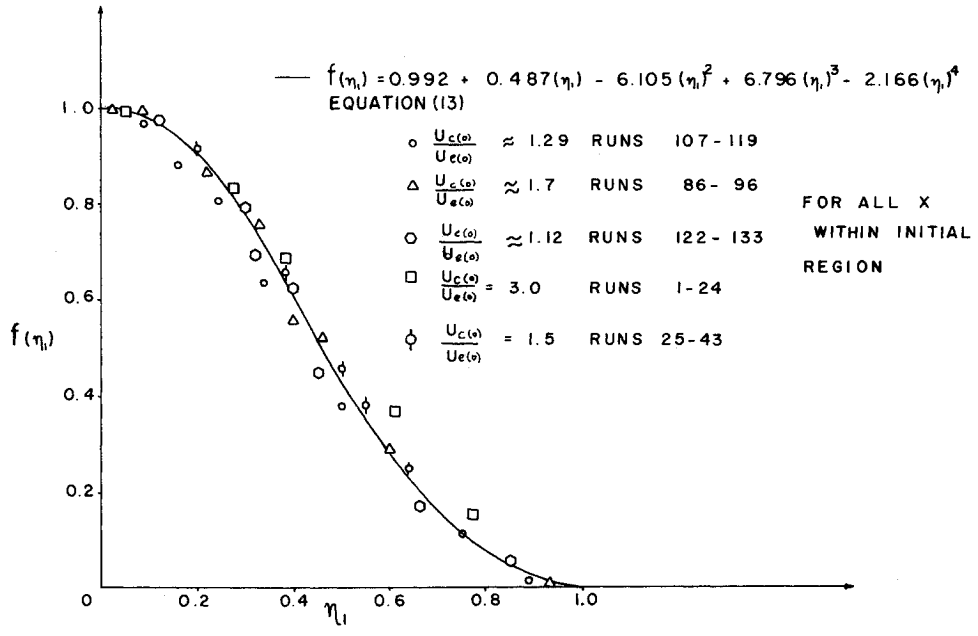

Fig. 9 Similarity for jet-layer velocity profiles in the initial region.

which is approximately 10 to 20 slot heights. The conditions at the end of the initial region such as wall layer momentum thickness, form factor, jet layer thickness, wake layer thickness, etc., vary with the velocity ratio $U_{c(0)}/U_{e(0)}$ at slot exit and pressure distribution. The distance downstream of slot exit up to which the minimum velocity point is observed increases as the initial velocity ratio approaches the value of one. At lower values of initial velocity ratio $U_{c(0)}/U_{e(0)}$ of 1.12 and 1.29, the velocity profile becomes that of an ordinary turbulent boundary shown in Figs. 3 and 4, respectively. Incipient separation occurs for $U_{c(0)}/U_{e(0)} = 1.12$, as seen from the velocity profile in Fig. 3. The existence of incipient separation was also verified by observation of movements of tufts that were attached to the flap surface. At higher values of initial velocity ratio, a wall-jet type of velocity profile still exists at the end of the flap, as seen in Fig. 5.

Figure 6 shows the relation between the quotient $\delta^{**}/\theta = \tilde{H}$ and the thickness ratio $H = \delta^*/\theta$. This figure shows that all velocity profiles for the wall layer in the initial and main region constitute a one-parameter family, and the same is true for velocity profiles when the viscous flow becomes of the ordinary boundary-layer type. The relationship between H and $\tilde{H}$ for the wall layer in the initial and main regions is given by

$$H = 4.411 - 23.9/\tilde{H} + 33.11/\tilde{H}^2 \quad (6)$$

whereas the relationship between H and $\tilde{H}$ when the viscous flow becomes of the ordinary turbulent boundary-layer type is given by

$$H = 16.133 - 56.91/\tilde{H} + 54.54/\tilde{H}^2 \quad (7)$$

Both of the preceding expressions have been obtained from experimental data by least-square curve fit. Figure 6 also shows the points obtained from experimental results by Rotta[20,10] for ordinary turbulent boundary layers. Figure 6 also shows values calculated from the expression

$$H = \tilde{H}/(3\tilde{H} - 4) \quad (8)$$

The foregoing relation can be derived with the assumption of power-law velocity profile.

Figure 7 shows a plot of $\tau_w/\frac{1}{2}\rho U_m^2$ vs momentum thickness Reynolds number $R_{e\theta}$, for various values of form factor. This figure indicates a peculiar characteristic of skin friction for wall-jet type of flow in that it increases with momentum thickness Reynolds number for constant value of form factor up to the point where the peak velocity disappears and the boundary-layer profile becomes of the ordinary turbulent boundary-layer type. Downstream of the point where the profile becomes of the ordinary boundary-layer type, the wall shear decreases with increasing momentum thickness Reynolds number for constant value of the form factor. For comparison, in the ordinary turbulent boundary-layer region the points calculated from the Ludwieg-Tillman[10] skin expression are shown plotted for various momentum thickness Reynolds numbers for constant values of the form factor. It is seen that the present indirect calculation of wall shear from the velocity profile is in good agreement with experimental skin friction law in the region where the wall-jet velocity profile has changed to an ordinary turbulent boundary-layer profile.

Figure 8 shows a plot of turbulent dissipation in the wall layer plotted as a function of local wall layer momentum thickness Reynolds number with form factor H as the parameter. These curves display characteristics similar to the wall shear, i.e., the value of the turbulent dissipation increases with local wall layer momentum thickness Reynolds number as long as a wall-jet type of velocity profile is present downstream of slot exit. This holds true for any initial velocity ratio at slot exit and pressure distribution. The magnitude of the turbulent dissipation then decreases with Reynolds number when velocity profile in the viscous region is of the ordinary boundary-layer type. Experimental data of Rotta for turbulent dissipation are shown as a band that includes velocity profiles having varying form factors.

Figure 8 shows the difference between wall shear and shear at a distance y above the wall, where the velocity is a maximum, vs wall layer momentum thickness Reynolds number. These curves illustrate that the shear at the maximum velocity point, when correlated with the usual parameter, does give good correlation. Analytical expressions have been obtained for the values of wall shear, turbulent dissipation for the wall layer, and difference of shear between the wall and the edge of wall layer. These expressions have been calculated by means of least-square fit of the points calculated from experimental velocity profiles and known pressure distribution. These expressions are as follows:

$$\tau_w/1/2\rho U_m^2 = 1.964 \exp[-1.819H + 35.68 \ln(R_{e\theta}) - 1.365\{\ln(R_{e\theta})\}^2][\ln(R_{e\theta})]^{-114.6} \times 10^{16}$$

$$= \text{wall skin-friction coefficient} \quad (9)$$

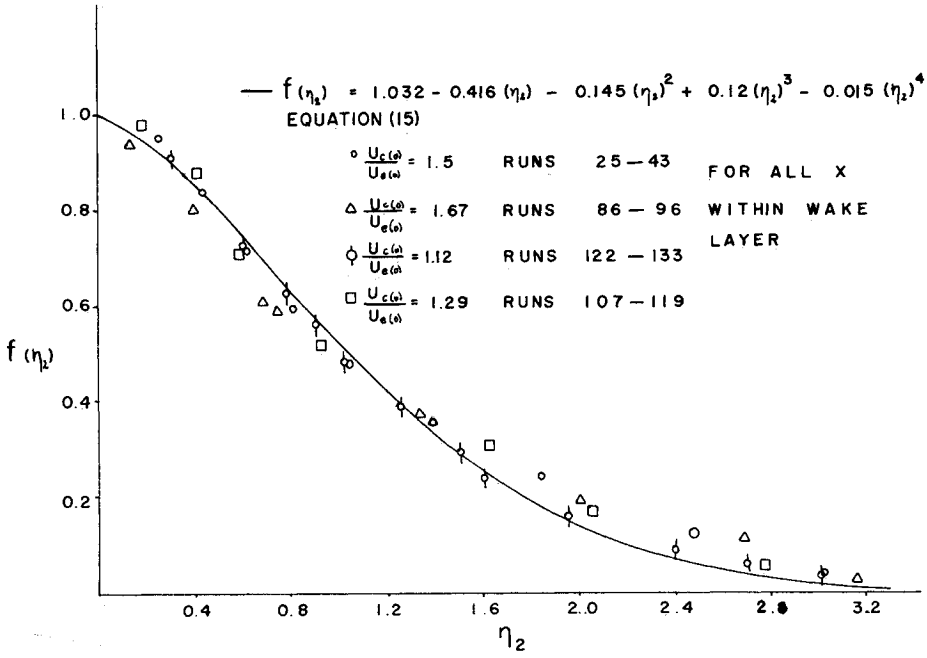

Fig. 10 Similarity for wake-layer velocity profiles in the initial region.

$$\int \frac{\tau}{1/2\rho U_m{}^2} \frac{\partial}{\partial y}\left(\frac{u}{U_m}\right) dy = 1.616 \exp[-0.636H + 48.55 \ln(R_{e\theta}) - 1.82\{\ln(R_{e\theta})\}^2] [\ln(R_{e\theta})]^{-158.7} \times 10^{23}$$

= wall-layer turbulent dissipation (10)

$$[\tau_w - \tau_{(\delta 5)}]/1/2\rho U_m{}^2 = 2.518 \exp[-0.918H + 17.21 \ln(R_{e\theta}) - 0.743\{\ln(R_{e\theta})\}^2] \times [\ln(R_{e\theta})]^{-45.79}$$

= difference between shear stress at the wall and at the edge of wall layer (11)

Figures 9–12 are nondimensional plots of velocity profiles obtained from experimental velocity profile data in initial and main regions. Experimental points shown in these figures are for various conditions at the slot exit as well as for different pressure distributions and different X locations.

Figure 9 shows the similarity of velocity profiles for the jet layer in the initial region. The similarity parameter and similarity function are defined as follows:

$$\eta_1 = (\delta_3 - y)/(\delta_3 - \delta_2)$$
$$f(\eta_1) = (U_c - u)/(U_c - U_w) \quad (12)$$

The least-square polynominal expression for $f(\eta_1)$ is given by the following expression:

$$f(\eta_1) = 0.992 + 0.487(\eta_1) - 6.105(\eta_1)^2 + 6.796(\eta_1)^3 - 2.166(\eta_1)^4 \quad (13)$$

Figure 10 shows the curve for the similarity of velocity profiles for the wake layer in the initial region. The similarity parameter and functions are, respectively, defined as

$$\eta_2 = (y - \delta_3)/(y_{1c} - \delta_3)$$
$$f(\eta_2) = (U_e - u)/(U_e - U_w) \quad (14)$$

where y_{1c} is the distance y in the wake layer where $f(\eta_2) = 0.5$. The least-square polynomial expression for $f(\eta_2)$ is given by

$$f(\eta_2) = 1.032 - 0.416(\eta_2) - 0.145(\eta_2)^2 + 0.12(\eta_2)^3 - 0.015(\eta_2)^4 \quad (15)$$

Figures 11 and 12 are the similarity curves for velocity profiles in the main region for the jet and wake layer, respectively. The definitions of similarity functions and parameters are the same as in the case of the initial region. The

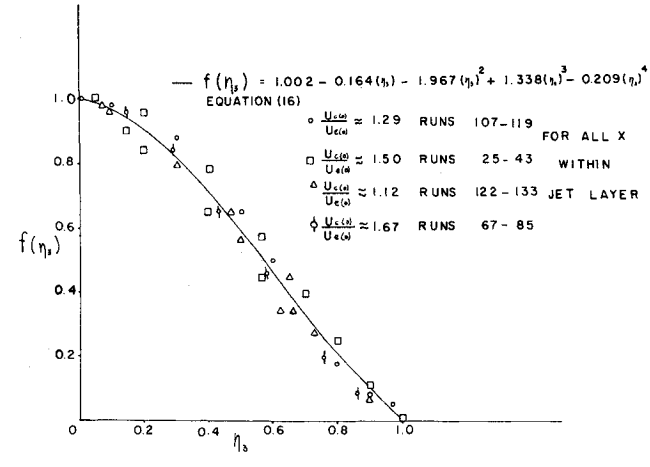

Fig. 11 Similarity for jet-layer velocity profiles in the

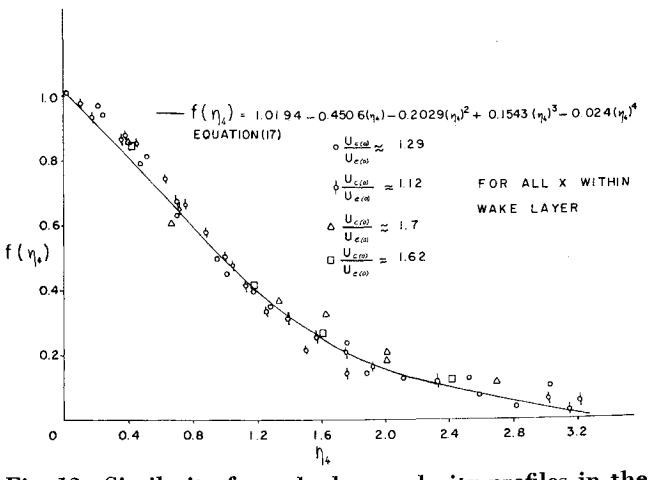

Fig. 12 Similarity for wake-layer velocity profiles in the

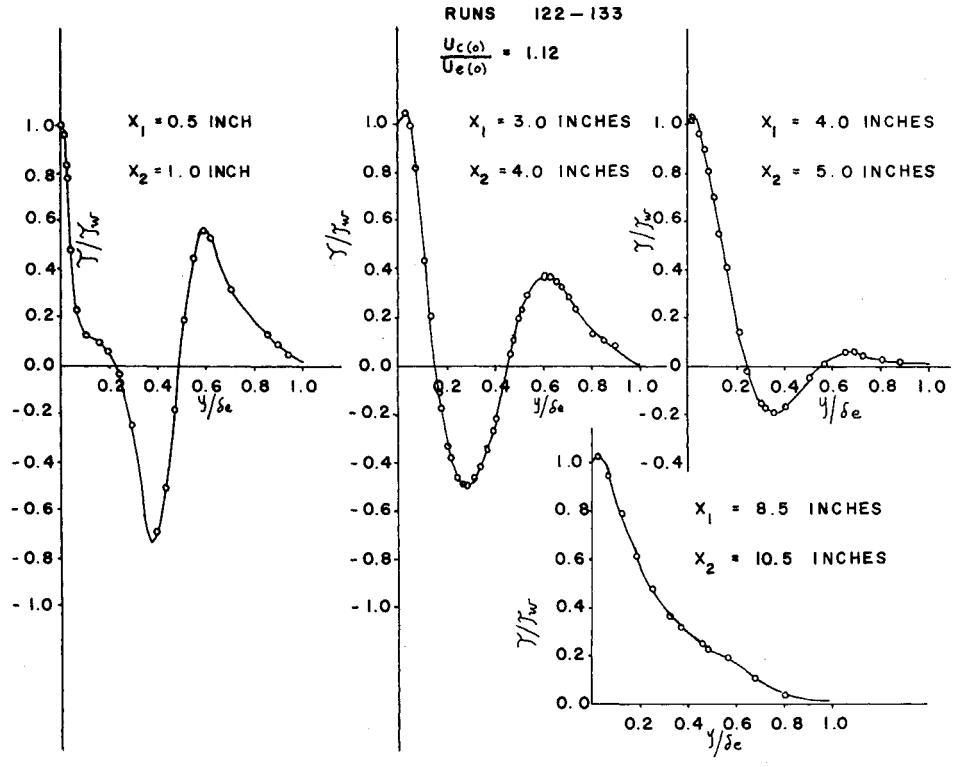

Fig. 13 Shear distribution for initial velocity ratio of 1.12.

least-square polynomial fit in the main region for the jet layer is

$$f(\eta_3) = 1.002 - 0.164(\eta_3) - 1.967(\eta_3)^2 + 1.338(\eta_3)^3 - 0.209(\eta_3)^4 \quad (16)$$

and for the wake region is

$$f(\eta_4) = 1.0194 - 0.450(\eta_4) - 0.2029(\eta_4)^2 + 0.1543(\eta_4)^3 - 0.024(\eta_4)^4 \quad (17)$$

It is apparent by comparing the similarity curves for the wake layer in the initial region and main region that the difference between these two curves is slight as compared to that between the similarity curves for the jet layer in the initial region and main region. It is also important to notice that the experimental data for different velocity ratios at slot exit and for different pressure distributions and X locations fall very nicely on a single curve when the similarity parameters are chosen as mentioned previously. It is this fact that facilitates the transformation of Prandtl's

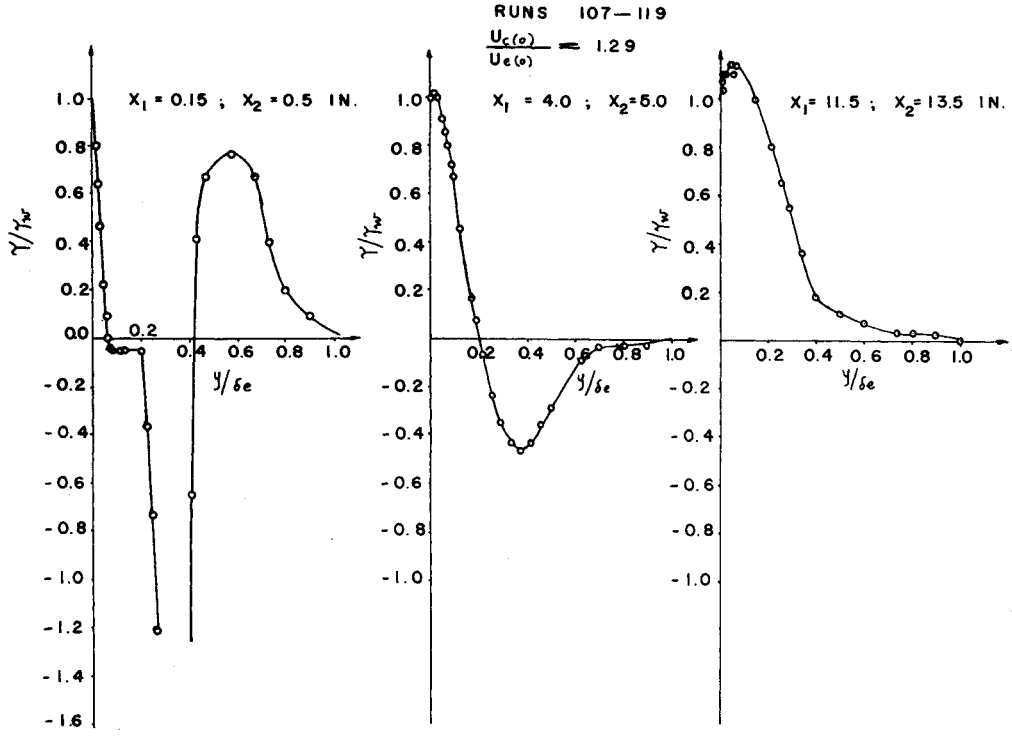

Fig. 14 Shear distribution for initial velocity ratio of 1.29.

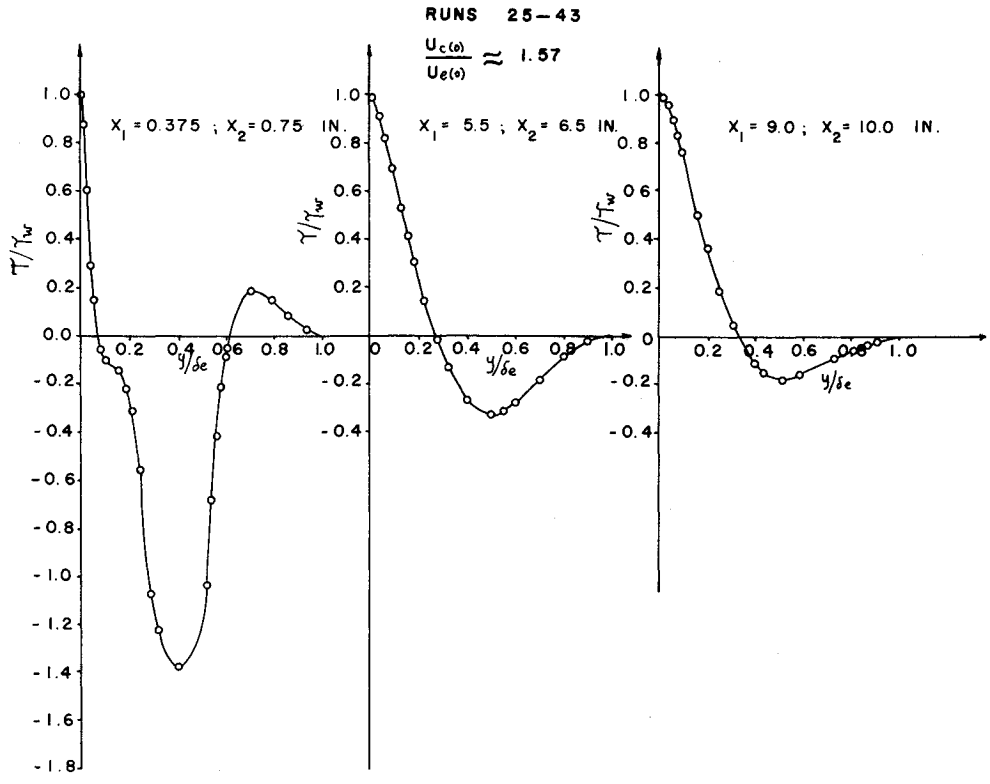

Fig. 15 Shear distribution for initial velocity ratio of 1.57.

boundary-layer partial differential equations[9,11] into ordinary differential equations that are amenable to solutions by the numerical techniques.

Figures 13–15 show plots of shear distributions in the viscous layer from the wall to the edge of the viscous region where shear stress is zero. These figures are for different initial velocity ratios and different pressure distributions. These curves are calculated from the experimental velocity profiles and pressure distributions. They are similar in shape and characteristics to those measured by various investigators such as Kacker and Whitelaw,[6,18] Kruka and Eskinazi,[2] and Bradshaw and Gee.[1] A few salient features observed from these calculated curves can be pointed out. The value of the shear stress changes sign in the neighborhood of the edge of the wall layer. The maximum value of the negative shear stress which is reached in the neighborhood of the wall layer depends greatly upon whether the X location is in the initial region or main region or in the ordinary turbulent boundary-layer region. The value of negative shear stress is maximum for X locations in the initial region and progressively decreases as the distance from slot exit increases. It can also be observed that the value of the shear stress in the viscous layer at the junction of jet and wake layer changes in sign from negative to positive. The shear stress in the core of the initial region remains approximately constant and near a value of zero.

Conclusions

As a result of the work described in this paper, some conclusions may be drawn:

1) Similarity of velocity profiles in the jet and wake layer is observed based on certain similarity parameters and variables. This holds true even in the presence of different pressure gradients.

2) Wall-layer velocity profiles can be represented as a one-parameter family as in the case of normal turbulent boundary layers.

3) Wall shear and wall-layer shear dissipation integral can be generalized as a function of local wall-layer momentum thickness Reynolds number and form factor as in the case of ordinary turbulent boundary layers.

4) Shear at peak velocity at the edge of the wall layer can be adequately correlated when $(\tau_w - \tau_{\delta 5})/\frac{1}{2}\rho U_m^2$ is expressed as a function of $U_m\theta/\nu$ and H.

5) A correlation between H and $\tilde{H}$ for the wall layer in the main and initial regions was found, but the correlation curve is different from that of ordinary turbulent boundary-layer velocity profiles.

6) The distance downstream from slot exit for which the wake layer exists is strongly dependent upon the initial velocity ratio at slot exit. This distance increases when the ratio $U_{c(0)}/U_{e(0)}$ approaches a value of one from either side.

7) The length of the initial region is approximately 7 to 15 slot heights, depending upon pressure gradient and initial conditions at slot exit.

References

[1] Bradshaw, P. and Gee, M. T., "Turbulent Wall Jets with and without an External Stream," Rept. 22, 008, June 1960, NASA.

[2] Kruka, V. and Eskinzai, S., "The Wall Jet in a Moving Stream," *Journal of Fluid Mechanics*, Vol. 20, Pt. 4, 1964.

[3] Meyers, G. E., Schauer, J. J., and Eustis, R. H., "Plane Turbulent Wall Jet Flow Development and Friction Factor," *Journal of Basic Engineering*, Vol. 85, March 1963, pp. 47–54.

[4] Hubbart, J. E. and Bangert, L. H., "Turbulent Boundary Layer Control by a Wall-Jet," AIAA Paper 70-107, New York, 1970.

[5] Hartnett, J. P., Birkebak, R. C., and Eckert, E. R. G., "Velocity Distributions, Temperature Distributions, Effectiveness and Heat Transfer for Air Injected through a Tangential Slot into a Turbulent Boundary Layer," *Journal of Heat Transfer*, Vol. 83, Aug. 1961, pp. 293–306.

[6] Kacker, S. C. and Whitelaw, J. H., "Some Properties of the Two Dimensional Turbulent Wall Jet in a Moving Stream," *Journal of Applied Mechanics*, Vol. 35, Dec. 1963, pp. 641–651.

[7] Patel, R. P. and Newman, B. G., "Self Preserving Two-Dimensional Turbulent Wall Jets in a Moving Stream," Rept. Ae. 5, 1961, McGill Univ., Montreal, Canada.

[8] Glauert, M. B., "The Wall Jet," *Journal of Fluid Mechanics*, Vol. 1, 1956, p. 625.

[9] Townsend, A. A., *The Structure of the Turbulent Shear Flow*, Cambridge University Press, 1956.
[10] Schlichting, H., *Boundary Layer Theory*, 4th ed., McGraw-Hill, New York, 1960.
[11] Abramovich, G. N., *The Theory of Turbulent Jets*, MIT Press, Cambridge, Mass., 1963.
[12] Sigalla, A., "Measurements of Skin Friction in a Plane Turbulent Wall Jet," *Journal of Royal Aeronautical Society*, Vol. 62, Dec. 1958, pp. 873–877.
[13] MacMillan, F. A., "Experiments on Pitot-tubes in Shear Flow," R&M 3028, 1957, NASA.
[14] Clauser, F. H., "The Turbulent Boundary Layer," *Advances in Applied Mechanics*, Vol. IV, Academic Press, New York, 1954.
[15] Seban, R. A. and Back, L. H., "Effectiveness and Heat Transfer for a Turbulent Boundary Layer with Tangential Injection and Variable Free-Stream Velocity," *Journal of Heat Transfer*, Vol. 84, Aug. 1962, pp. 235–244.
[16] Escudier, M. P. and Whitelaw, J. H., "The Influence of Strong Adverse Pressure Gradients on the Effectiveness of Film Cooling," *International Journal of Heat and Mass Transfer*, Vol. 11, Aug. 1968, pp. 1289–1292.
[17] Nicoll, W. B. and Whitelaw, J. H., "The Effectiveness of the Uniform Density, Two-Dimensional Wall Jet," *International Journal of Heat and Mass Transfer*, Vol. 10, 1967, pp. 623–639.
[18] Kacker, S. G. and Whitelaw, J. H., "The Turbulence Characteristics of Two-Dimensional Wall-Jet and Wall-Wake Flows," Paper 70-WA/APM-35, American Society of Mechanical Engineers.
[19] Seban, R. A. and Back, L. H., "Velocity and Temperature Profiles in a Wall Jet," *International Journal of Heat and Mass Transfer*, Vol. 3, 1961, pp. 255–265.
[20] Rotta, J., "Schubspannungsverteilung und Energiedissipation bei Turbulenten Grenzschichten," *Ingeniur Archiv*, Vol. 20, 1952, pp. 195–207.

NOVEMBER 1971 AIAA JOURNAL VOL. 9, NO. 11

Fuel Droplet Burning Rates in a Combustion Gas Environment

G. M. Faeth* and R. S. Lazar†
The Pennsylvania State University, University Park, Pa.

Measurements were made of droplet burning rates in the combustion products of a flat flame burner at atmospheric pressure. Various alcohols and paraffins were tested at ambient temperatures from 1660°K to 2530°K and ambient oxygen concentrations in the range 0–37%. Existing theories of droplet combustion (when corrected for flame zone dissociation) gave an adequate prediction of the variation in burning rate with changes in the ambient temperature and oxygen concentration. However, the theories progressively overestimated the burning rate as the fuel molecular weight increased, with errors as high as 50% for the heavier hydrocarbons.

Nomenclature

a,b = constants in the expression $C_p = a + bT$
C_p = specific heat at constant pressure
d = droplet diameter
H_c = heat of reaction of liquid fuel and gaseous oxidizer
K = burning rate constant
$\dot{m}$ = mass evaporation rate
Pr = Prandtl number
Re = Reynolds number
Sc = Schmidt number
t = time
T = temperature
V = gas velocity
Y_x = effective ambient oxygen mass fraction
γ_o = ratio of the stoichiometric mass flow rate of oxygen to fuel
Δl = fuel heat of vaporization
λ = thermal conductivity
ρ = liquid density

Subscripts

l = droplet surface
o = pertains to no-flow conditions
∞ = ambient conditions

Introduction

BECAUSE of its importance as an elemental process in the combustion of sprays, many investigators have studied the burning of single fuel droplets. Most of these studies were conducted by burning droplets at low-ambient temperatures with oxygen concentrations ranging from air to pure oxygen. Studies of droplet combustion in an environment more representative of combustion chamber conditions, however, have been much more limited.

Wood et al.[1] considered the droplet combustion of hexadecane, kerosene and a number of heating oils within a gaseous premixed flame. Droplet burning was observed for oxygen mass fractions in the range 0–0.81. The gas temperature was kept constant at 1775°K. Average burning rate constants were inferred from measurements of the initial droplet diameter and the total time of combustion luminosity. This technique is of limited accuracy, however, due to uncertainties in the relationship between the start and end of combustion luminosity and the start and end of the steady burning period.

Ingebo[2] has made measurements of ethanol evaporation rates in a rocket engine combustion chamber and Bolt et al.[3] considered the combustion of a number of hydrocarbons in a burning spray. However, the state of the gas surrounding the droplets in these experiments was not sufficiently well-defined to allow comparison of the results with theoretical predictions of droplet burning rates.

The present study provides more extensive measurements of droplet burning rates at high-ambient temperatures. The droplets were subjected to the combustion products of a flat flame burner at atmospheric pressure. The burner was operated with various gas compositions to yield temperatures in the range 1660–2530°K and oxygen mass fractions in the range 0–0.37, at the droplet location. The fuels considered in the study included methyl, 1-butyl and 1-decyl alcohol as well as the paraffin hydrocarbons n-pentane, n-heptane, iso-octane, n-decane, n-tridecane, and n-hexadecane.

Received June 19, 1970; revision received June 16, 1971. Supported in part under NASA Grant NGR 39-009-077.

* Associate Professor of Mechanical Engineering. Member AIAA.
† Research Assistant. Associate Member of AIAA.